Granular Matter (2019) 21:107
https://doi.org/10.1007/s10035-019-0958-7

ORIGINAL PAPER

Granular scale responses in the shear band region

Hu Zheng[1,2,3,4] · Dong Wang[3] · Xinmeng Tong[3,5] · Lihui Li[3,6] · Robert P. Behringer[3]

Received: 20 February 2019 / Published online: 29 October 2019

Abstract
The essence of macroscopic shear band phenomena is the cumulative cooperation of granular scale particle rearrangements. In this work, we report an experimental study to present the granular scale properties as the shear band is generated in a confined granular material with soft boundaries. The photoelastic experimental technique is applied to illuminate the force chain network in our experiments. Particle scale stresses are extracted from the photoelastic response. Meanwhile, other particle scale performances like displacements and rotation are also detected. According to the distribution of particle scale volumetric strain, the shear band region and the state of bifurcation are well defined. We find that pressure inside of each particle does not have a clear correlation with the shear band region. Conversely, the local density variation and particle rotation have strong correlation with the shear band region.

Keywords Shear band · Photoelastic experiments · Granular materials · Local density · Particle rotation

1 Introduction

Granular materials are ubiquitous in nature and also one of the most prevalent materials in industry which have attracted much scientific attention recently [1–5]. Granular materials can flow as liquids and behave as solids [6–10]. The stability of the granular materials is one of the most important problems that attract interest from scientists and engineers. The failure of geogranular materials can induce natural hazards like landslides and avalanches [11, 12] which have been widely reported [3, 13]. The deformations within granular materials under external loading are mostly concentrated in shear bands [14], where the granular failure is usually located.

In the past few decades, tremendous theoretical, numerical, and experimental works have been reported on the fundamental mechanisms of granular localized failure [1, 15–19]. Zheng and Li [20] proposed a phenomenological theory to model shear banding, shear band propagation, and branching on mesoscopic scales by using the Ginzburg–Landau formalism. The model is able to capture shear localization (banding), shear band propagation and branching, and crack propagation and its velocity in the deformation process. Zhao and Li [21] developed a constitutive theory on deviation of shear band inclination angles in bulk metallic glasses which is based mainly on the Drucker–Prager model and a free-volume theory. Du Bernard et al. [13] reported the localized increase in porosity or dilation in shear band for poorly consolidated sand based on their experimental study. Borja et al. [22] conducted a plane strain compression test on a rectangular sand specimen combining with X-ray Computed Tomography (CT) technique, and found that spatial density variation could be a determining factor for the selection of the persistent shear band in a symmetrically

This article is part of the Topical Collection: In Memoriam of Robert P. Behringer.

✉ Dong Wang
dong.wang@yale.edu

[1] Department of Geotechnical Engineering, College of Civil Engineering, Tongji University, Shanghai 200092, China

[2] Key Laboratory of Geotechnical and Underground Engineering of Ministry of Education, Tongji University, Shanghai 200092, China

[3] Department of Physics and Center for Non-linear and Complex Systems, Duke University, Durham, NC 27708, USA

[4] School of Earth Science and Engineering, Hohai University, Nanjing 211100, Jiangsu, China

[5] Department of Physics and Astronomy, Johns Hopkins University, 3400 N. Charles Street, Baltimore, MD 21218, USA

[6] Institute of geology and geophysics, Chinese Academy of sciences, Beijing 100029, China

loaded localizing sand body. However, most of the previous works focused on the macroscopic performances in the shear band region during the granular deformation process. At this point, there is relatively little experimental work that directly address the connections among the granular scale performances in the shear band region. The goal of the present work is to gain a preliminary understanding the correlation of these granular scale parameters in the deformation process.

In this work, a uniaxial compression experiment is conducted on a pressure confined two-dimensional granular system based on the photoelastic technique. The photoelastic experimental method allows tracking individual granular force information in the shear band generating process [23–25] . We define shear band regions based on the distribution of particle scale volumetric strain. Meanwhile, the local density, granular rotation, and individual particle pressure information are presented to reveal the granular scale performances in the shear band regions.

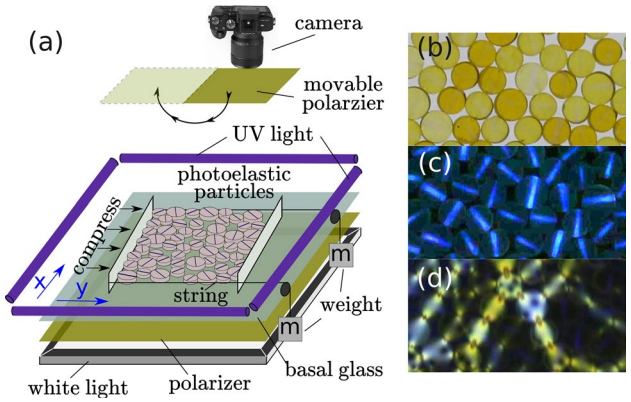

Fig. 1 (Color online) **a** 3D schematic of the experimental apparatus. A moving-wall compresses (indicated by the arrows) bidisperse photoelastic particles by 1 mm steps. The confining pressure is provided by two strings, which can be adjusted by the hinging weight through two pulling. Each particle is marked a UV-fluorescent ink bar on the top surface, which can be used to tracking particle orientation at each step. At each step, the system is imaged in white light without polarizer, **b** to locate the particle position, in UV light, **c** to tracking the particle orientation, and with polarizer, **d** to calculate the force information

2 Experimental protocol

We applied the photoelastic technique in our experiments, which has proved to as a effective experimental method in granular materials research [7, 25–27]. The photoelastic response is based on the birefringence properties of double refractive index (DRI) materials. However, in otherwise optically isotropic materials, the external load can also cause stress induced birefringence. There is a linear constitutive equation to relate the local stress to the birefringence (Eq. 1) which can be used to compute the local stress inside the material.

$$n_1 - n_2 = C(\sigma_1 - \sigma_2) \tag{1}$$

where n_1 and n_2 are the principle indices of refraction coinciding with the principal stress directions, C is the stress-optic coefficient, and σ_1 and σ_2 are the eigenvalues of the stress tensor.

The experimental apparatus, as sketched in Fig. 1a, consists of a $\mathrm{W} \times \mathrm{L} = 200 \times 395\,\mathrm{mm}^2$ compression cell confined by two strings and two rigid walls. The granular sample, which is a mixture of 1357 bidisperse (1019 small and 338 large) two-dimensional photoelastic disks. We avoid the crystal packing by well mixing the bidisperse particles in the compression cell. The diameters of big and small particles are 8.76 mm and 7.44 mm, respectively. The initial packing fraction (ϕ_{ini}) is approximately 81.86%. The confining pressure of the granular sample in our experiments can be tuned by the string tension. The data presented in this work is collected by hanging 580 g weight to provide the confining pressure. One of the rigid walls is fixed, while the other one is driven by a stepper motor to compress the granular sample quasi-statically. Each step has magnitude $\Delta = 1$ mm, which is corresponding to $\gamma = \frac{\Delta}{L} \approx 0.25\%$ strain. After each step, the system can be illuminated by the circularly polarized white light from below or by ultraviolet (UV) lights from above. The patterns of the granular sample illuminated by different light sources can be recorded by a high-resolution camera (Canon EOS 70D, $5472 \times 3648 px^2$).

We take three pictures for each compression step. The first one is taken while the granular sample is illuminated by the white light (Fig. 1b), which is called the *white light image*. The spatial location of each particle can be located based on the white light image. When the white light is turned off with the UV light on, the camera can take an image like Fig. 1c. Because we marked a small UV-fluorescent ink bar on the surface of each photoelastic particle, only the UV bars are illuminated by the UV light. Hence, each particle orientation can be detected from these UV bars. The polarized image is taken with another movable circular polarizer in front of the camera, as shown in Fig. 1d. The photoelastic response of the granular sample can be visualized while particles have force contacts with their neighbours. The bearing pressure, P, of each particle can be calculated from the squared intensity gradient by the polarized image. The pressure $P \propto \overline{G^2} =< |\nabla I|^2 >$ [23–25], where I is the intensity of the polarizer image, and G^2 indicates the average gradient squared of intensity over the whole particle region. We repeat the experiments five times to collect data, which presents similar shear band profiles. Here, we choose one of the trials to discuss the granular scale response in the shear band region.

3 Results and discussions

3.1 Shear band region

Associated with any affine displacement or deformation in a local region, the non-affine motion is considered as the part which leads to irreversibility or plasticity—the shear band generation [2]. The spatial density variation is usually accompanied by shear band generation. Falk and Langer [28] fitted local granular motion occurring over a time δt to an affine motion. They defined a mean square difference between the actual distances from the neighbor particles to the central particle and the ones as if particles followed a certain strain field, $D^2(t, \delta t)$, while the local uniform strain tensor, ε_{ij}, can be calculated by minimizing $D^2(t, \delta t)$, which is referred to as D^2_{min}. More details about how to calculate the local uniform strain tensor, ε_{ij}, and D^2_{min} can refer to [28]. Meanwhile, volumetric strain, ε_v, is extracted from ε_{ij} and is an important parameter to present the granular scale density variation during compression. Beside the local large shear strain region, the emergence of local low density region is another essential signal for detecting the shear band. Many X-ray experiments on sand indicate that the shear band is the percolation of the local low density region [29, 30]. Hence, we choose ε_v for defining shear band, which also has a strong correlation to the local shear strain, ε.

Figure 2a shows the probability distribution function PDF(ε_v) of each shear step; the color map indicates the shear strain (γ is from 0 to 10.89%). The volumetric strain of each particle indicates the local density changing during shear. Positive values of ε_v mean dilation, while negative values indicate compression. The PDFs of ε_v are similar to Gaussian distribution with the peaks are nearly 0 at small shear strain steps. The peak of PDF(ε_v) shifts to negative value as the shear strain increases, but the tail of the distribution function become longer. The peak position of PDF(ε_v) fluctuates around -0.015 when the shear strain increases beyond approximately 5% (inset of Fig. 2a), which indicates that local dilation of granular system starts at $\gamma = 5\%$. The average of volumetric strain, $\langle \varepsilon_v \rangle$, as a function of strain (Fig. 2b) shows that the slope of $\langle \varepsilon_v \rangle$ versus γ curve turns to positive from negative, which also indicates the system starts to dilate locally as the strain increases beyond 5%. However, the variation of global packing fraction with the strain (Inset of Fig. 2b) does not follow the same trend as $\langle \varepsilon_v \rangle$. One would expect local ϕ to increase when ε is negative. However, Fig. 2b-inset shows that the global ϕ decreases to a value smaller than that at the beginning after the strain is more than 4%, when ε is still negative. This can be understood as a result of having a higher pressure than that at strain 0. In addition,

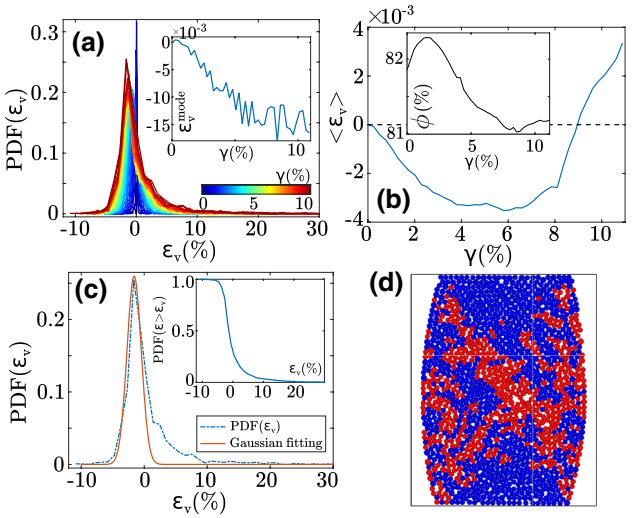

Fig. 2 (Color online) **a** The probability distribution function PDF(ε_v) for each shear step from $\gamma = 0\%$ to 10.89%. Inset: the peak position of PDF(ε_v) as a function of shear strain, γ. **b** the average of volumetric strain, $\langle \varepsilon_v \rangle$, as a function of γ. Inset: the global volume fraction versus γ. **c** The PDF(ε_v) at $\gamma = 10.89\%$ and the Gaussian distribution function fitting curve. Inset: complementary cumulative distribution function as a function of ε_v. **d** The shear band region defined at $\gamma = 10.89\%$ by the PDF(ε_v); red particles are the particle in the defined shear band region

this observation, together with the main part of Fig. 2b, suggest a highly local region of dilation when shear band occurs.

The initial packing fraction of the granular sample is less than the isotropic jamming packing fraction. Hence, the average of ε_v is negative immediately, caused by the compression at the first couple of steps of shearing. However, the average of ε_v increases as the shear strain increases due to the Reynolds dilation [31, 32], which also can be considered as the moment when the shear band is starting to develop. The changing of average of ε_v which is calculated at the granular scale is consistent with the microscopic volume changing of classic triaxial tests in soil mechanics studies [33, 34].

The PDF(ε_v) at the maximum shear strain in this experiment is shown in Fig. 2c, which is the final state of this experiment. Comparing with initial symmetric PDF(ε_v), an asymmetric tail on the right side of the distribution shows up because of particle scale dilation during shear. The distribution no longer well follow a Gaussian distribution, which could be fitted better with a non-Gaussian distribution. However, we assume the asymmetric tail is actually the dilating particles in the shear band region. Hence, we fit the PDF(ε_v) by the Gaussian distribution function here, which is the solid pink curve in Fig. 2c, and pick the dilating particles to define the shear band region in this granular system. The Gaussian fitting was performed by *Nonlinear least squares* method.

In practice, we choose the half width ($\sigma = 0.015 \pm 0.001$) as the cutoff for identifying particles within the shear band. Figure 2d shows the spatial distribution of the particles in the shear band region which is defined by the tail of Gaussian distribution. The particles in the shear band region are plotted in red, while not are plotted in blue. A clear **X** shape region with approximately 5–7 particle diameters width [35] can be observed from Fig. 2d, which is connected by the red particles. Many researchers have reported this **X** geometry shear band region in previous work on granular and soil triaxial experiments [3, 36, 37]. Hence, we believe the shear band definition based on the ε_v distribution is robust. From Fig. 2d, we can find some gaps in the shear band region, which represent the low-local packing fraction caused by ε_v dilation. In the following section, the local density variation will be discussed in detail.

3.2 Local force and density variation

One of the advantages of the photoelastic technique is that we can extract particle scale forces from the polarized image [23–25]. Figure 3a–d show local force and density variation at different shear strains. The diameter of each particle indicates the pressure inside of the particle and the force chain network inside of the granular system. Red circles represent particles in the shear band region, and blue circles represent particles outside of the shear band region. The pressure of particles in the shear band region is not necessarily higher or lower than the particle pressures outside of shear band region. Thus, we do not observe a clear correlation between the particle pressure and shear band region here. The strong force chains usually coincide with the compression direction

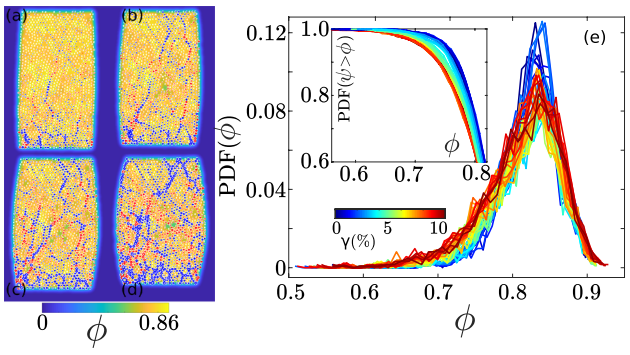

Fig. 3 (Color online) **a**–**d** The coarse grained density of the granular system at the different shear strain, $\gamma = 2.53\%, 5.06\%, 7.59\%$ and 10.89%, respectively. The red and blue circles indicate the position of each particle; red particles are in the shear band region, and blue particles are not in the shear band region. The diameter of the circle indicates the bearing pressure of the particle (Arbitrary Unit), which is calculated from the photoelastic response of the particle in the polarized light field. **e** The probability distribution function of Voronoi cell fraction. The color map indicates the shear strain, which is from 0% to 10.89%. Inset: the cumulative distribution of Voronoi cell fraction

as shown in Fig. 3a–d, however, the shear band does not necessarily form along the compression direction. This might be the reason why there is no clear correlation observed here.

Conversely, the local density variation should have strong correlation with the shear band. The spatial density variation of a granular system can be calculated based on the coarse-grained method, which has been introduced in detail by Zhang et al. [38] and Clark et al. [39]. The coarse-grained density maps of the granular system at different shear strains are shown in Fig. 3a–d. A low density region is created at $\gamma = 5.06\%$, which indicates the shear band starts to develop. This is consistent with the average ε_v signal (Fig. 2b). The local low density regions increase as the shear strain increases and connect together as the shear band region.

The Voronoi Diagram is applied to quantitatively analyze the particle scale density [40, 41]. The scale density can be defined as:

$$\phi_i = \frac{\pi r_i^2}{V_i} \tag{2}$$

where r_i is the radius of the particle i, and V_i is the area of the corresponding Voronoi cell. Figure 3e shows the probability distribution function of local packing fraction PDF(ϕ) for the different shear strain, $\gamma = 0\%$ to 10.89%. Here, we did not take the boundary particle into account to calculate the particle scale ϕ distribution due to the abnormal Voronoi cell area. The peak position of PDF(ϕ) is always near the isotropic jamming point, $\phi_J \approx 84\%$. The width of the distribution increases as the shear strain increases, because the system is dilating as the shear band develops. This shear induced low particle scale density can also be observed from the complementary cumulative distribution function (Inset of Fig. 3b). We can see here that the shear band development is highly correlated with the particle scale density variation.

3.3 Particle rotation

Circular particles can rotate in a frictional granular system. In our system, the orientation of each particle can be tracked based on the UV ink on the surface of each particle, that can be illuminated by UV light. The difference of the particle orientations at different compression steps is defined as the particle rotation compared with the initial orientations. Figure 4 shows the particle rotation at different shear strain, where the particle position is marked as circles with the diameter indicating the magnitude of rotation compared with the initial state. Red circles represent shear band region particles, and blue circles represent particles that are not in the shear band region. The particles with high rotation magnitude are mostly located in the shear band region or

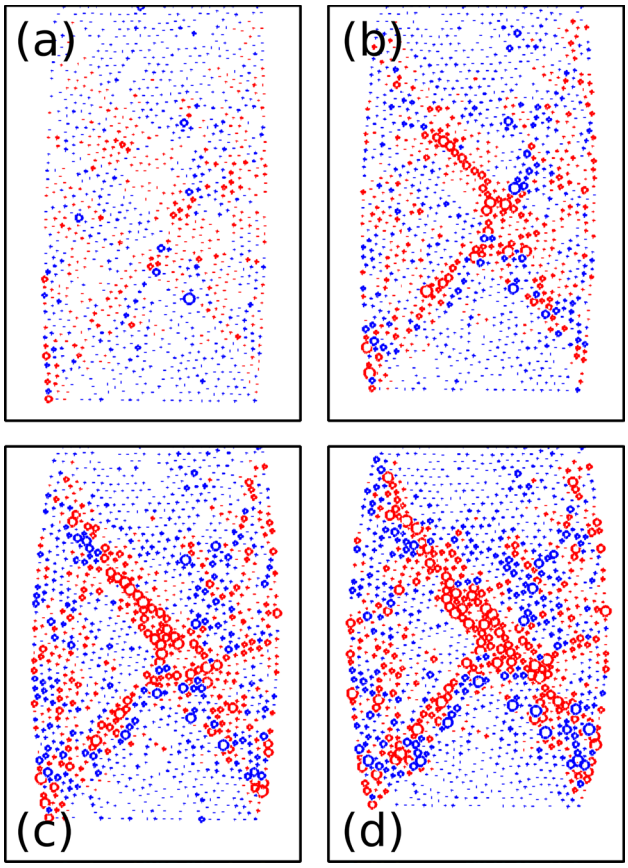

Fig. 4 (Color online) The rotation of each particle at the different shear strain: (**a**) $\gamma = 2.53\%$, (**b**) $\gamma = 5.06\%$, (**c**) $\gamma = 7.59\%$, and (**d**) $\gamma = 10.89\%$. The red and blue circles indicate the position of each particle, red particles are the particle in the shear band region. The diameter of the circle means rotation magnitude, the biggest diameter represents *pi* / 2 rotation

the boundary of the shear band region. The particle rotations show high correlation to the region of the shear band.

4 Conclusions

In this work, we study the particle scale performance in a granular shear band region by using 2D photoelastic particles. We first extract the shear band region based on the PDF(ε_v). The photoelastic technique allows for the direct extraction of particle scale force information in the granular system. We find that there is no clear correlation between the particle pressures and the location of shear band region. On the other hand, the spatial density variation in the granular sample has a strong correlation with the shear band region. The low-density spots are usually in the shear band region. Moreover, the particles with high rotation magnitude are always located in the shear band region.

Acknowledgements This work is dedicated to Bob Behringer, whom we are deeply indebted to and will forever miss. His role in supporting and mentoring this research clearly justifies inclusion as a coauthor. Discussions with Ryan Kozlowski, Aghil Abed Zadeh, Cacey Stevens Bester, David Chen, Yiqiu Zhao and Yuchen Zhao are highly appreciated. HZ acknowledges the support from NSFC(41672256) and NSFC(Jiangsu) (BK20180074). This work was funded by NSF Grant No. DMR1206351 and DMR1809762, ARO No. W911NF-18-1-0184, NASA Grant No. NNX15AD38G, the William M. Keck Foundation, RT-MRSEC fellowship (DW).

Compliance with ethical standards

Conflict of interest The authors declare that they have no conflict of interest.

References

1. Tang, H., Zhang, X., Ji, S.: Discrete element analysis for shear band modes of granular materials in triaxial tests. Part. Sci. Technol. **35**(3), 277–290 (2017)
2. Utter, B., Behringer, R.P.: Experimental measures of affine and nonaffine deformation in granular shear. Phys. Rev. Lett. **100**(20), 208302 (2008)
3. Veveakis, E., Stefanou, I., Sulem, J.: Failure in shear bands for granular materials: thermo-hydro-chemomechanical effects. Géotech. Lett. **3**(2), 31–36 (2013)
4. Zheng, H., Wang, D., Barés, J., Behringer, R.P.: Sinking in a bed of grains activated by shearing. Phys. Rev. E **98**(1), 010901 (2018)
5. Zheng, H., Wang, D., Chen, D.Z., Wang, M., Behringer, R.P.: Intruder friction effects on granular impact dynamics. Phys. Rev. E **98**, 032904 (2018)
6. Wang, D., Ren, J., Dijksman, J.A., Zheng, H., Behringer, R.P.: Microscopic origins of shear jamming for 2d frictional grains. Phys. Rev. Lett. **120**, 208004 (2018)
7. Bi, D., Zhang, J., Chakraborty, B., Behringer, R.P.: Jamming by shear. Nature **480**(7377), 355 (2011)
8. Zheng, H., Dijksman, J.A., Behringer, R.P.: Shear jamming in granular experiments without basal friction. Europhys. Lett. **107**(3), 34005 (2014)
9. Jaeger, H.M., Nagel, S.R., Behringer, R.P.: Granular solids, liquids, and gases. Rev. Mod. Phys. **68**(4), 1259 (1996)
10. Ohern, C.S., Silbert, L.E., Liu, A.J., Nagel, S.R.: Jamming at zero temperature and zero applied stress: the epitome of disorder. Phys. Rev. E **68**(1), 011306 (2003)
11. Yu, H., Weijie, Z., Qiang, X., Pan, X., Liang, H., (2012) Run-out analysis of flow-like landslides triggered by the ms 8.0 Wenchuan earthquake using smoothed particle hydrodynamics. Landslides **9**(2), 275–283 (2008)
12. Huang, Y., Cheng, H.: A simplified analytical model for run-out prediction of flow slides in municipal solid waste landfills. Landslides **14**(1), 99–107 (2017)
13. Bernard, X.D., Eichhubl, P., Aydin, A.: Dilation bands: A new form of localized failure in granular media. Geophys. Res. Lett. **29**(24), 29–1 (2002)
14. Bardet, J.P., Proubet, J.: Shear-band analysis in idealized granular material. J. Eng. Mech. **118**(2), 397–415 (1992)
15. Desrues, J., Andò, E.: Strain localisation in granular media. C. R. Phys. **16**(1), 26–36 (2015)
16. Guo, P.: Critical length of force chains and shear band thickness in dense granular materials. Acta Geotech. **7**(1), 41–55 (2012)

17. Xue-Ying, J., Wan-Huan, Z., Hua-Xiang, Z., Zhen-Yu, Y., Yang-min, L.: On the interface shearing behavior between granular soil and artificial rough surfaces. In: Advances in Laboratory Testing and Modelling of Soils and Shales, pp. 437–444. Springer (2017)
18. Xiaoqing, G., Huang, M., Qian, J.: Dem investigation on the evolution of microstructure in granular soils under shearing. Granul. Matter **16**, 91–106 (2014)
19. Xiaoqing, G., Jing, H., Huang, M.: Anisotropy of elasticity and fabric of granular soils. Granul. Matter **19**, 33 (2017)
20. Zheng, G.P., Li, M.: Mesoscopic theory of shear banding and crack propagation in metallic glasses. Phys. Rev. B **80**(10), 104201 (2009)
21. Zhao, M., Li, M.: A constitutive theory and modeling on deviation of shear band inclination angles in bulk metallic glasses. J. Mater. Res. **24**(8), 2688–2696 (2009)
22. Borja, R.I., Song, X., Rechenmacher, A.L., Abedi, S., Wu, W.: Shear band in sand with spatially varying density. J. Mech. Phys. Solids **61**(1), 219–234 (2013)
23. Howell, D., Behringer, R.P., Veje, C.: Stress fluctuations in a 2d granular couette experiment: a continuous transition. Phys. Rev. Lett. **82**(26), 5241 (1999)
24. Geng, J., Behringer, R.P.: Slow drag in two-dimensional granular media. Phys. Rev. E **71**(1), 011302 (2005)
25. Majmudar, T.S., Behringer, R.P.: Contact force measurements and stress-induced anisotropy in granular materials. Nature **435**(7045), 1079 (2005)
26. Zhao, Y., Zheng, H., Wang, D., Wang, M., Behringer, R.P.: Particle scale force sensor based on intensity gradient method in granular photoelastic experiments. New J. Phys. **21**(2), 023009 (2019)
27. Zadeh, A.A., Barés, J., Brzinski, T.A., Daniels, K.E., Dijksman, J., Docquier, N., Everitt, H., Kollmer, J.E., Lantsoght, O., Wang, D., et al.: Enlightening force chains: a review of photoelasticimetry in granular matter. Granul. Matter **21**, 13 (2019)
28. Falk, M.L., Langer, J.S.: Dynamics of viscoplastic deformation in amorphous solids. Phys. Rev. E **57**(6), 7192 (1998)
29. Oda, M., Takemura, T., Takahashi, M.: Microstructure in shear band observed by microfocus x-ray computed tomography. Geotechnique **54**(8), 539–542 (2004)
30. Alshibli, K.A., Hasan, A.: Spatial variation of void ratio and shear band thickness in sand using x-ray computed tomography. Géotechnique **58**(4), 249–257 (2008)
31. Reynolds, O.: Lvii. On the dilatancy of media composed of rigid particles in contact. With experimental illustrations. Lond. Edinb. Dublin Philos. Mag. J. Sci. **20**(127), 469–481 (1885)
32. Ren, J., Dijksman, J.A., Behringer, R.P.: Reynolds pressure and relaxation in a sheared granular system. Phys. Rev. Lett. **110**(1), 018302 (2013)
33. Barnes, G.: Soil Mechanics: Principles and Practice. Macmillan International Higher Education, London (2016)
34. Ting, J.M., Corkum, B.T., Kauffman, C.R., Greco, C.: Discrete numerical model for soil mechanics. J. Geotech. Eng. **115**(3), 379–398 (1989)
35. Veje, C.T., Howell, D.W., Behringer, R.P.: Kinematics of a two-dimensional granular couette experiment at the transition to shearing. Phys. Rev. E **59**, 739–745 (1999)
36. Khidas, Y., Jia, X.: Probing the shear-band formation in granular media with sound waves. Phys. Rev. E **85**(5), 051302 (2012)
37. Rechenmacher, A.L.: Grain-scale processes governing shear band initiation and evolution in sands. J. Mech. Phys. Solids **54**(1), 22–45 (2006)
38. Zhang, J., Behringer, R.P., Goldhirsch, I.: Coarse-graining of a physical granular system. Prog. Theor. Phys. Suppl. **184**, 16–30 (2010)
39. Clark, A.H., Mort, P., Behringer, R.P.: Coarse graining for an impeller-driven mixer system. Granul. Matter **14**(2), 283–288 (2012)
40. Brandt, J.W., Algazi, V.R.: Continuous skeleton computation by voronoi diagram. CVGIP: Image Underst. **55**(3), 329–338 (1992)
41. Kise, K., Sato, A., Iwata, M.: Segmentation of page images using the area voronoi diagram. Comput. Vis. Image Underst. **70**(3), 370–382 (1998)